JACS
JOURNAL OF THE AMERICAN CHEMICAL SOCIETY
Article
pubs.acs.org/JACS

Light-Emitting Superstructures with Anion Effect: Coordination-Driven Self-Assembly of Pure Tetraphenylethylene Metallacycles and Metallacages

Xuzhou Yan,*[,†] Ming Wang,[‡] Timothy R. Cook,[§] Mingming Zhang,[†] Manik Lal Saha,[†] Zhixuan Zhou,[†] Xiaopeng Li,[‡] Feihe Huang,*[,∥] and Peter J. Stang*[,†]

[†]Department of Chemistry, University of Utah, 315 South 1400 East, Room 2020, Salt Lake City, Utah 84112, United States
[‡]Department of Chemistry and Biochemistry, Texas State University, San Marcos, Texas 78666, United States
[§]Department of Chemistry, University at Buffalo, 359 Natural Sciences Complex, Buffalo, New York 14260, United States
[∥]State Key Laboratory of Chemical Engineering, Center for Chemistry of High-Performance & Novel Materials, Department of Chemistry, Zhejiang University, Hangzhou 310027, PR China

Supporting Information

ABSTRACT: Herein, we describe the synthesis of tetraphenylethylene (TPE)-based di-Pt(II) acceptors as shown by X-ray analysis, which are subsequently used to construct pure TPE-based 2D hexagonal metallacycles and 3D drumlike metallacages with three different counteranions via coordination-driven self-assembly. The metallacycles possess alternating TPE donor and acceptor units that arrange 12 pendant phenyl rings along the outer perimeter that provide the basis for the observed aggregation-induced emission (AIE) behavior. The metallacages are similarly constructed from TPE-based building blocks, specifically two donors and four acceptors, resulting in eight freely rotating phenyl rings decorating the prismatic core. The fluorescence of these cages in dilute solution is intensified when hexane is added to CH_2Cl_2 solutions, indicative of aggregation-induced enhanced emission (AIEE). The influence of the counteranions on the photophysics of the assemblies was investigated. The molar absorption coefficients (ε), fluorescence emission intensities, and quantum yield (Φ_F) values of the SCCs with different counteranions in CH_2Cl_2 follow the order PF_6^- > OTf^- > NO_3^-. The same trend also applies to the AIE characteristics of the SCCs in the aggregated state. The metal−organic materials developed here not only enrich a newly emerging library of self-assembly AIE metallacycles and cages that are promising candidates for turn-on fluorescent sensors and advanced optical devices but also provide an understanding of how structural factors affect the photophysics of AIE-active SCCs.

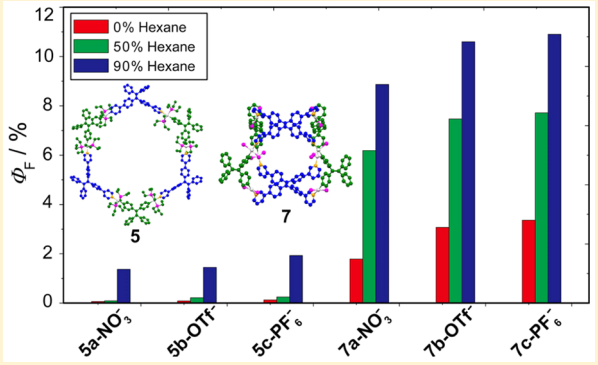

INTRODUCTION

The ongoing search for highly efficient fluorescent materials is motivated by their widespread application as imaging agents and sensors, components of light-emitting diodes, and data recording and storage, among others.[1] However, traditional fluorophores often suffer from aggregation-caused quenching in condensed states that limits their practical applications in settings where high concentrations or solid materials are necessary. In 2001, a phenomenon known as aggregation-induced emission (AIE) was introduced by Tang and co-workers, wherein chromophores that undergo nonradiative decay through intramolecular rotations/vibrations in dilute solutions emit brilliant fluorescence upon molecular aggregation.[2] A well-known AIE-active fluorophore is TPE in which twisting of the C=C bond and rotations of the phenyl rings are suppressed when aggregated, thereby shutting down nonradiative relaxation pathways and enabling emission.[3] Recently, AIE-active molecules have been adapted as building blocks in supramolecular frameworks to define a strategy to realize fluorescence that is not predicated on molecular packing effects.[4] The development of structurally complex supramolecular architectures with light-emitting properties directly benefits the applications mentioned above and introduces optical properties and functions that complement existing fluorophores.

Coordination-driven self-assembly, which is based on the spontaneous formation of metal−ligand bonds, has emerged as a well-established method to construct discrete supramolecular coordination complexes (SCCs) with predictable shapes and sizes, such as 1D helices, 2D polygons, and 3D polyhedra.[5] The well-defined cavities and ease with which functional groups may

Received: January 24, 2016
Published: March 16, 2016

DOI: 10.1021/jacs.6b00846
J. Am. Chem. Soc. 2016, 138, 4580−4588

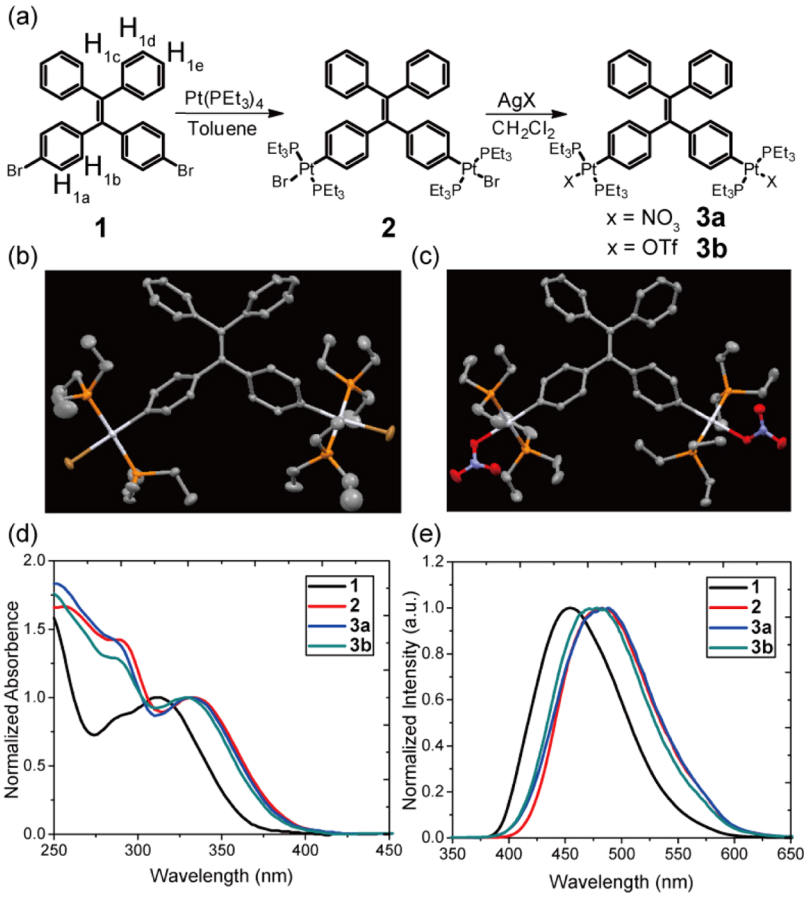

Figure 1. (a) Synthesis of TPE-based di-Pt(II) acceptor **3**. Crystal structures of (b) **2** and (c) **3a**. Hydrogen atoms are omitted for clarity. Thermal ellipsoids are drawn at 50% probability level. Normalized (d) absorption (CH_2Cl_2) and (e) emission (solid state, λ_{ex} = 330 nm) spectra of **1**−**3**.

be installed onto the periphery of SCCs have rendered them applicable in encapsulation, catalysis, supramolecular polymerization, and so on.[6] Very recently, light-emitting metal−organic materials based on SCC platforms have captured much attention because of their potential for applications in materials science and biotechnology.[7] However, the influence of structure (metal-coordination modes, counteranions, and geometries) on the light-emitting properties of metal−organic materials is an elusive yet intriguing issue.

The construction of structurally versatile and complex pure TPE superstructures is attractive because coordination-driven self-assembly of TPE-containing precursors into SCCs results in new photophysical features that are not observed for the free TPE subcomponents.[2,3] In this work, we report the design and construction of the first metallacycles and metallacages wherein both the donor and acceptor building blocks contain AIE molecules: a TPE-based di-Pt(II) organometallic precursor and TPE-based dipyridyl or tetrapyridyl ligands. Although the metallacycles show weak fluorescent emission under dilute conditions, the metallacages fluoresce strongly. Upon molecular aggregation, both the metallacycles and cages exhibit typical AIE characteristics with markedly increased quantum yields (Φ_F) attributed to a restriction of the rotation of the pendant phenyl rings. A counterion effect was observed, revealing that species containing OTf^- or PF_6^- counterion give rise to stronger emission than their NO_3^- counterions analogues.

RESULTS AND DISCUSSION

The TPE-based di-Pt(II) acceptors were synthesized in two steps starting from dibromo-TPE precursor **1**. The oxidative addition of **1** to $Pt(PEt_3)_4$ at each bromide site furnished **2** after which the bromide ligands were exchanged by treatment with $AgNO_3$ or AgOTf to give **3a** or **3b**, respectively (Figure 1a). The two variants of **3** were characterized by a suite of spectroscopic techniques (Figures S10, S14, and S33). The structures of **2** and **3a** were unambiguously determined by single-crystal X-ray diffraction (Figure 1b,c). The normalized absorption and emission spectra of **1**−**3** are shown in Figure 1d,e. Compound **1** displayed a broad absorption band centered at 310 nm. After oxidative addition, the lowest energy band moderately red-shifted ca. 23 nm in the spectrum of **2**. Upon ion exchange, the lowest energy bands of **3a** and **3b** underwent minor blueshifts (Figure 1d). In dilute solutions, compounds **1**−**3** do not emit because of their innate torsional conformations. However, they fluoresce in the solid state with bands centered at 454 nm for **1**, 482 nm for **2**, 483 nm for **3a**, and 477 nm for **3b** (Figure 1e).

With TPE-based di-Pt(II) acceptor in hand, we first synthesized [3 + 3] metallacycles **5a** and **5b** by stirring a mixture of ligand **4** with **3a** or **3b**, respectively, in a 1:1 ratio in CD_2Cl_2 at room temperature for 8 h (Figure 2a). **5c** was obtained by the addition of a saturated aqueous solution of KPF_6 into an acetone solution of **5b** to exhange counteranions (Scheme S4). The formations of **5a**−**c** were investigated by NMR analyses (^1H and ^{31}P) of the reaction mixtures. The

DOI: 10.1021/jacs.6b00846
J. Am. Chem. Soc. 2016, 138, 4580−4588

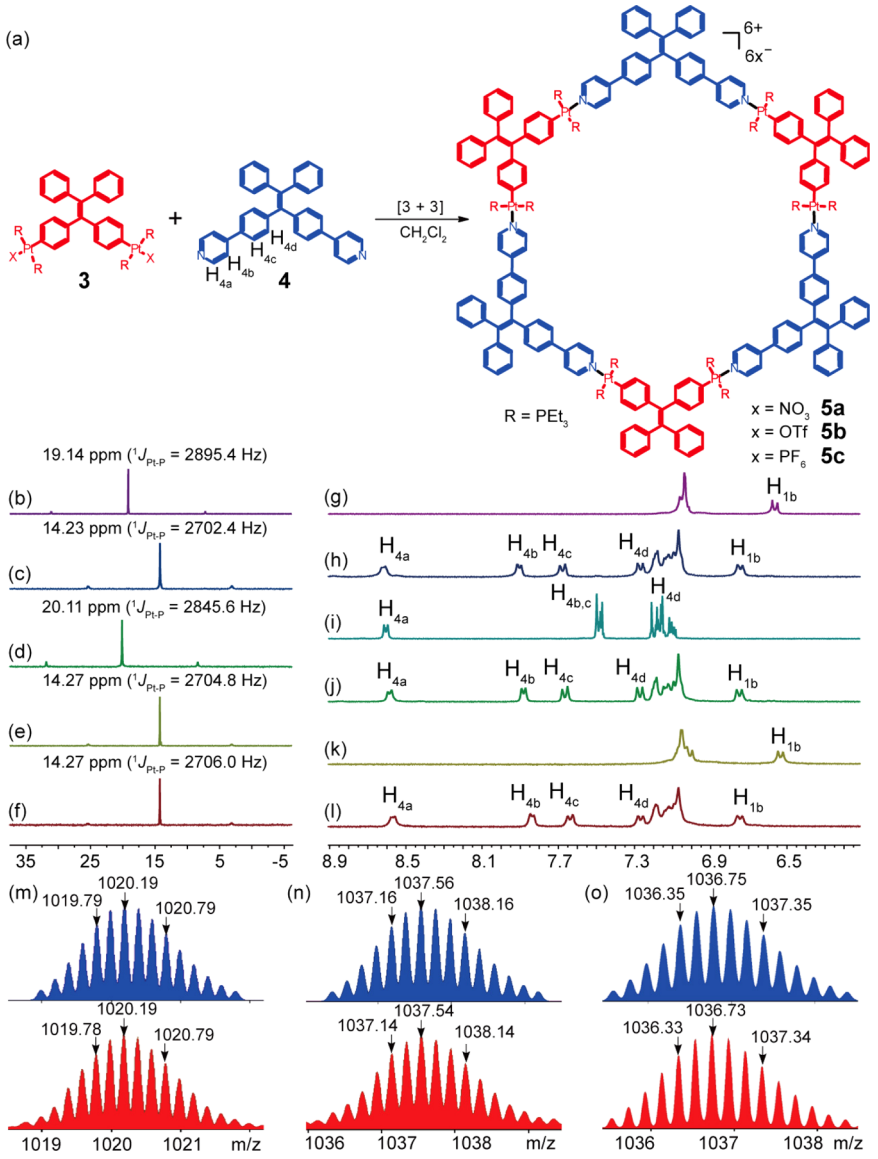

Figure 2. (a) Self-assembly of **3** with **4** to give **5**. Partial $^{31}P\{^{1}H\}$ (b–f) and ^{1}H NMR (g–l) spectra (300 MHz, CD_2Cl_2, 293 K) of **3a** (b and g), **3b** (d and k), **4** (i), **5a** (c and h), **5b** (e and j), and **5c** (f and l). Experimental (red) and calculated (blue) ESI-TOF-MS spectra of **5a** $[M - 5NO_3]^{5+}$ (m), **5b** $[M - 5OTf]^{5+}$ (n), and **5c** $[M - 5PF_6]^{5+}$ (o).

$^{31}P\{^{1}H\}$ NMR spectra of **5a–c** showed sharp singlets (ca. 14.2 ppm for **5a**, 14.3 ppm for **5b** and **5c**) shifted upfield from those of the corresponding starting di-Pt(II) acceptors **3a** and **3b** by ca. 4.91, 5.84, and 5.84 ppm, respectively (Figure 2, spectra b–f). In the ^{1}H NMR spectrum of **5a** (Figure 2, spectrum h), the protons of the pyridyl and phenyl rings exhibited downfield shifts relative to those of **4** ($\Delta\delta[H_{4b}]$ = 0.41 ppm, $\Delta\delta[H_{4c}]$ = 0.21 ppm, and $\Delta\delta[H_{4d}]$ = 0.12 ppm), consistent with coordination to Pt. Similar chemical shift changes were also observed for **5b** and **5c** (Figure 2, spectra j and l), indicating that the counterions have no obvious influence on the ^{1}H NMR signals of the assemblies. Electrospay ionization time-of-flight mass spectrometry (ESI-TOF-MS) provided further evidence for the formation of the metallacycles. In the ESI-TOF-MS spectra of **5a–c** (Figures S17, S20, and S23), peaks at m/z = 1020.19, 1037.54, and 1036.73, corresponding to $[M - 5NO_3]^{5+}$ for **5a** (Figure 2m), $[M - 5OTf]^{5+}$ for **5b** (Figure 2n), and $[M - 5PF_6]^{5+}$ for **5c** (Figure 2o), respectively, were observed. These peaks were isotopically resolved and in good agreement with their calculated theoretical distributions.

Having obtained pure TPE metallacycles, we set out to construct metallacages similarly decorated with TPE groups. Stirring a mixture of **3a** or **3b** with tetrapyridyl ligand **6** in a 2:1 ratio in DMSO-d_6 at 50 °C for 8 h resulted in the formation of [4 + 2] metallacages **7a** or **7b**, respectively (Figure 3a). The OTf^- anions of the cage **7b** were exchanged by treatment with a saturated aqueous solution of KPF_6 to yield **7c** (Scheme S7). The verification of the formation of discrete assemblies in the reaction mixtures was made by NMR (^{1}H and ^{31}P) and ESI-TOF-MS analyses. In the ^{1}H and $^{31}P\{^{1}H\}$ NMR spectra, all of the signals became broadened (Figures 3, spectra b–l), consistent with the formation of large constructs with tumbling motions that are slow on the NMR time scale. At high temperature, the signals became sharp (Figure S34). Moreover, the singlets in the $^{31}P\{^{1}H\}$ NMR spectra (Figure 3, spectra c, e, and f) and the unchanged number of signals in the aromatic regions of the ^{1}H NMR spectra (Figure 3, spectra h, j, and l) all

DOI: 10.1021/jacs.6b00846
J. Am. Chem. Soc. 2016, 138, 4580–4588

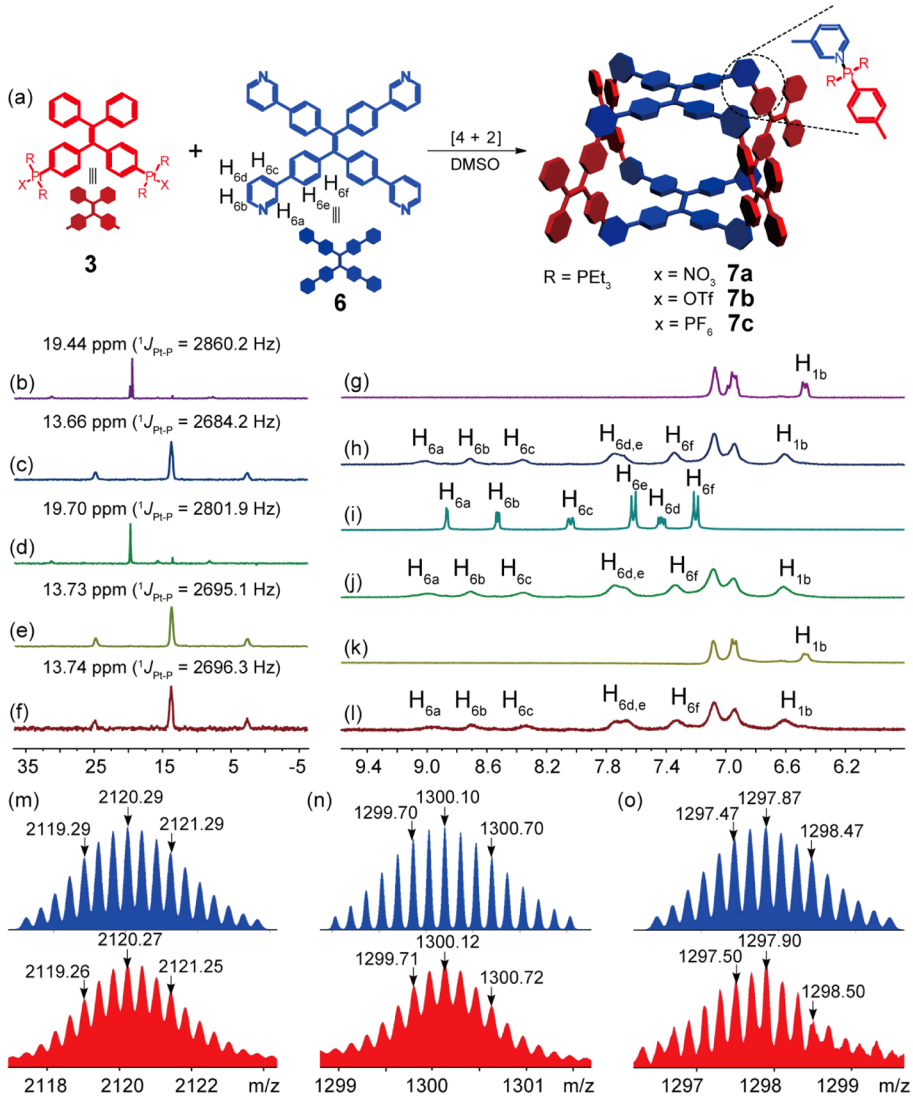

Figure 3. (a) Self-assembly of **3** with **6** to give **7**. Partial $^{31}P\{^{1}H\}$ (b–f) and ^{1}H NMR (g–l) spectra (300 MHz, DMSO-d_6, 293 K) of **3a** (b and g), **3b** (d and k), **6** (i), **7a** (c and h), **7b** (e and j), and **7c** (f and l). Experimental (red) and calculated (blue) ESI-TOF-MS spectra of **7a** $[M - 3NO_3]^{3+}$ (m), **7b** $[M - 5OTf]^{5+}$ (n), and **7c** $[M - 5PF_6]^{5+}$ (o). The impurity on spectra b and d is caused by DMSO-d_6 because it can coordinate with **3a** and **3b**.

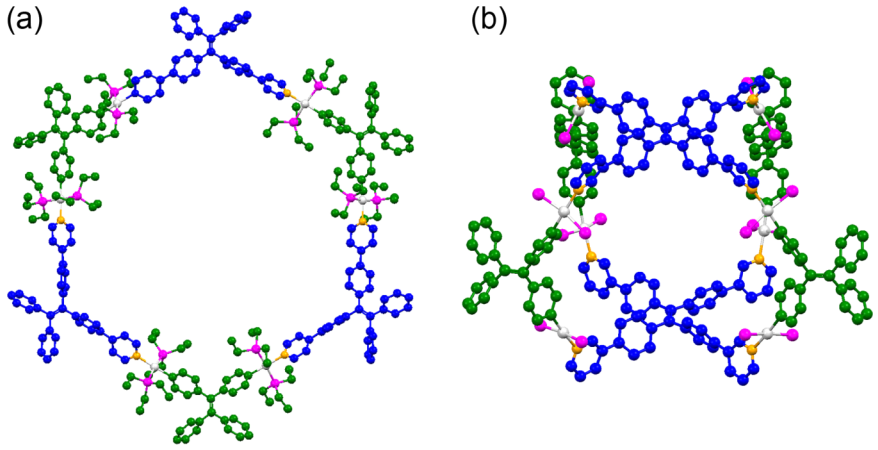

Figure 4. Simulated molecular models of (a) **5** and (b) **7** optimized by PM6 semiempirical molecular orbital methods.

suggest discrete and symmetrical structures. All of the proton signals of the pyridyl and phenyl rings (H_{a-f}) of **7a–c** shifted downfield, and their phosphorus signals displayed upfield shifts upon Pt–N coordination. The stoichiometry of formation of

DOI: 10.1021/jacs.6b00846
J. Am. Chem. Soc. 2016, 138, 4580–4588

the metallacages was further demonstrated by ESI-TOF-MS analysis. In their spectra, peaks corresponded to intact assemblies with charge states resulting from the loss of counterions, for example, m/z = 2120.27 attributable to $[M - 3NO_3]^{3+}$ for **7a** (Figure 3m), m/z = 1300.12 attributable to $[M - 5OTf]^{5+}$ for **7b** (Figure 3n), and m/z = 1297.90 attributable to $[M - 5PF_6]^{5+}$ for **7c** (Figure 3o), were observed. The isotopically resolved distributions agree with their calculated patterns.

Because of the difficulty of growing X-ray-quality single crystals of these assemblies, molecular simulations were employed to gain further insight into the structural characteristics of the metallacycles and metallacages. The simulated structure of **5** possessed a roughly planar hexagon core with alternating TPE donor and acceptor sites. This arrangement places 12 pendant phenyl rings along the periphery of the metallacycle (Figure 4a). Molecular simulation indicated that **7** adopted a drumlike tetragonal prismatic shape with two TPE ligands held in a cofacial arrangement with the eight exterior phenyl rings of the TPE acceptors aligned around the prismatic core (Figure 4b). The presence of these TPE moieties results in the unique photophysics associated with AIE (vide infra).

In the absorption spectra (Figure 5a), di-Pt(II) acceptors **3a** and **3b** showed similar broad absorption bands centered at 334 nm. Ligand **4** has a broad absorption band at 312 nm, and **6** has two broad absorption bands at 280 and 347 nm. After metal-coordination, **5a**, **5b**, and **5c** exhibited sharp absorption bands at 340, 344, and 342 nm with molar absorption coefficients (ε) of 1.50 × 10^5, 1.77 × 10^5, and 2.09 × 10^5 $M^{-1}cm^{-1}$, respectively. In the absorption spectra of the metallacages, sharp low energy bands at 332 nm with ε of 1.55 × 10^5 $M^{-1}cm^{-1}$ for **7a**, 1.70 × 10^5 $M^{-1}cm^{-1}$ for **7b**, and 1.85 × 10^5 $M^{-1}cm^{-1}$ for **7c** were observed.

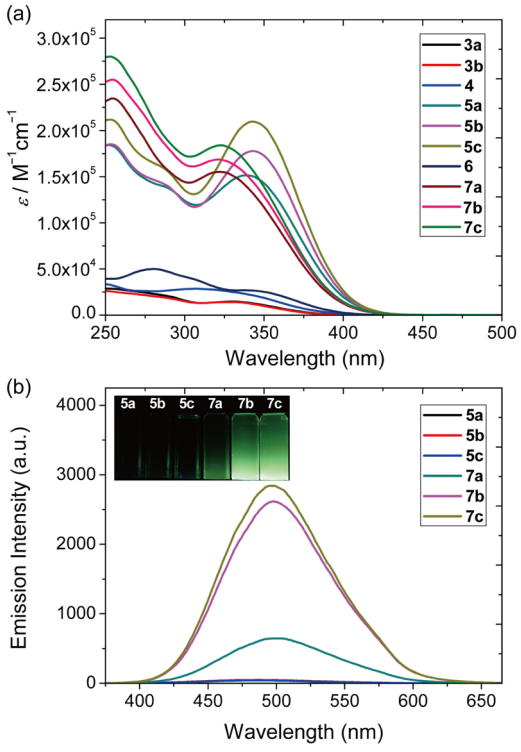

Figure 5. (a) Absorption and (b) fluorescence emission spectra of the building blocks and assemblies in CH_2Cl_2 (λ_{ex} = 350 nm, c = 10.0 μM). Inset: photograph of **5** and **7** in CH_2Cl_2 upon excitation at 365 nm using an UV lamp at 298 K (c = 10.0 μM).

The emission spectra of the assemblies are shown in Figure 5b. The emission of **5a**–**c** is weak at ca. 485 nm (inset of Figure 5b) likely due to nonradiative decay that occurs by rotations of the pendant phenyl rings. In sharp contrast, **7a**–**c** are strongly emissive at ca. 500 nm, which can be attributed to the locking of nonemissive TPE ligands within the rigid metallacages, specifically introduced from the donor building blocks. Notably, **7b** and **7c** showed 4.05- and 4.42-fold fluorescence enhancement over **7a** at 10.0 μM, respectively.

The emission spectra of the building blocks and the assemblies were determined in CH_2Cl_2 and CH_2Cl_2/hexane mixed solutions (Figures 6 and S35). The emission wavelengths and intensities of **3**, **4**, and **6** displayed no obvious changes in CH_2Cl_2/hexane mixtures due to their solubilities (Figure S35), showing that they are not AIE-active fluorophores in such mixed solvent systems. In mixed solutions with <60% hexane content, metallacycles **5a**–**c** emitted weakly (Figure 6a–c,g). Upon increasing the hexane content to 90%, marked emission enhancements were observed. The formation of aggregates at this percentage of hexane was demonstrated by the appearance of low-energy tailing bands in the absorption profiles of **5a**–**c** in CH_2Cl_2/hexane solutions (Figure S36a–c). Furthermore, these results support that the assemblies **5a**–**c** are AIE-active. In the 30–80% hexane content range, the emission intensities of both **5b** and **5c** were higher than that of **5a** (Figure 6g). Although **7a**–**c** fluoresce strongly in CH_2Cl_2, they still also show additional AIE enhancements (Figure 6d–f,h) because the phenyl rings of the acceptor fragments may be rigidified upon aggregation. For example, the emission intensities of **7a**–**c** gradually increased upon constant increase of the hexane fraction to 90% in mixed solutions. Moreover, across the entire mixed solvent range, both **7b** and **7c** exhibited a higher emission intensity than that of **7a** under the same conditions (Figure 6h). Scanning electron microscopy (SEM) of the SCCs was further carried out to demonstrate the formation of nanoaggregates in CH_2Cl_2/hexane mixed solutions with 90% hexane content (Figure 7). SCCs **5a**–**c** and **7a**–**c** were all formed into well-defined spherical nanoaggregates with average diameters between 150 and 250 nm. The morphologies of the obtained aggregates do not change significantly on the basis of geometry or counteranion. Therefore, the nonradiative decay processes of pendent phenyl rings on either metallacycles or metallacages were presumably suppressed by aggregation so as to induce clearly enhanced fluorescence.

The fluorescent characteristics of **5** and **7** in mixed solvent solutions could be further probed by changes in Φ_F values (Figure 8). In CH_2Cl_2, Φ_F values were determined to be 0.065% for **5a**, 0.093% for **5b**, 0.13% for **5c**, 1.79% for **7a**, 3.07% for **7b**, and 3.36% for **7c**. At a 90% hexane fraction, their Φ_F values reached 1.37, 1.45, 1.93, 8.87, 10.6, and 10.9%, respectively. It is noteworthy that the SCCs with PF_6^- counterions display the highest Φ_F values and those with NO_3^- counterions show the lowest Φ_F values both in solution and in the aggregated state. The Φ_F values follow the order PF_6^- > OTf^- > NO_3^-. These observations indicate the relative ability of each counteranion to influence the fluorescence emission of SCCs, reminiscent of the well-known Hofmeister effect wherein the nature of counterions effects the folding/unfolding and solubility of biomacromolecules.[8] As such, it is reasonable to expect that counterions may play a role in the photophysical properties of SCCs that incorporate AIE

DOI: 10.1021/jacs.6b00846
J. Am. Chem. Soc. 2016, 138, 4580–4588

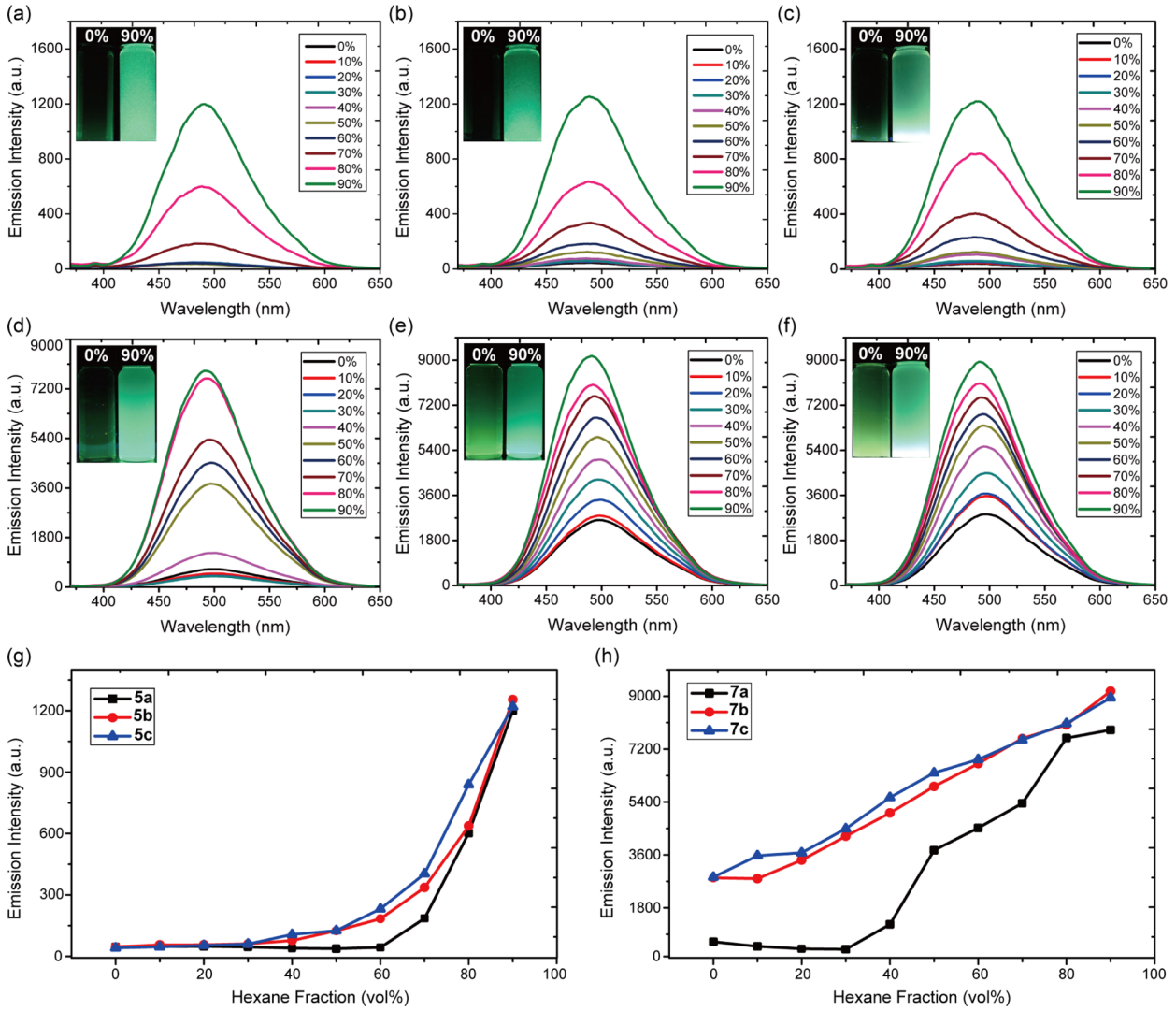

Figure 6. Fluorescence emission spectra and plots of maximum emission intensity of **5a** (a and g), **5b** (b and g), **5c** (c and g), **7a** (d and h), **7b** (e and h), and **7c** (f and h) versus hexane fraction in CH_2Cl_2/hexane mixtures (λ_{ex} = 350 nm, c = 10.0 μM). Insets: photographs of assemblies in CH_2Cl_2 and 10%/90% CH_2Cl_2/hexane mixture upon excitation at 365 nm using an UV lamp at 298 K (c = 10.0 μM).

molecules, particularly when they influence the solubility of the resulting metallacycles or cages.

CONCLUSIONS

We have demonstrated that the well-established directional-bonding methodology of coordination-driven self-assembly of predetermined subunits allows the facile construction of SCCs with unique photophysical properties. Specifically, novel TPE-based di-Pt(II) acceptors were designed and synthesized, from which six metallacycles and metallacages were prepared with high efficiency for the first time, thus enriching the library of light-emitting metal–organic materials. Photophysical studies reveal that the connection topology of the nonemissive TPE building blocks and counteranions associated with assemblies bring about distinct fluorescence emission. These observations provide an enhanced understanding of the impact of structural features on the photophysics of AIE-active superstructures, which opens up possibilities for the development of light-emitting metal–organic materials based on SCC platforms with potential applications in biotechnologies and molecular electronics.

EXPERIMENTAL SECTION

Materials and Methods. All reagents were commercially available and used as supplied without further purification. Deuterated solvents were purchased from Cambridge Isotope Laboratory (Andover, MA). Compounds **1**,[9] **4**,[7e] **6**,[10] and $Pt(PEt_3)_4$[11] were prepared according to the published procedures. NMR spectra were recorded on a Varian Unity 300 or 400 MHz spectrometer. ^{1}H and ^{13}C NMR chemical shifts are reported relative to residual solvent signals, and $^{31}P\{^1H\}$ NMR chemical shifts are referenced to an external unlocked sample of 85% H_3PO_4 (δ = 0.0). Mass spectra were recorded on a Synapt G2 ESI-Q-TOF mass spectrometer using electrospray ionization with a MassLynx software suite. The melting points were collected on a SHPSIC WRS-2 automatic melting point apparatus. The UV–vis experiments were conducted on a Hitachi U-4100 absorption spectrophotometer. The fluorescent experiments were conducted on a Hitachi F-7000 fluorescence spectrophotometer. Quantum yields were determined using quinine sulfate at 365 nm (Φ_F = 56%). The crystals data were collected on a Nonius KappaCCD diffractometer equipped with Mo KR radiation (λ = 0.71073 Å). SEM experiments were carried out on FEI Quanta 600 FEG.

Synthesis of ***2****.* A 50 mL Schlenk flask was charged under nitrogen with **1** (411 mg, 0.840 mmol) and $Pt(PEt_3)_4$ (1.40 g, 2.10 mmol). Freshly distilled toluene (40.0 mL) was added to the flask under nitrogen by syringe, and the resulting mixture was stirred for 72 h at 90

DOI: 10.1021/jacs.6b00846
J. Am. Chem. Soc. 2016, 138, 4580–4588

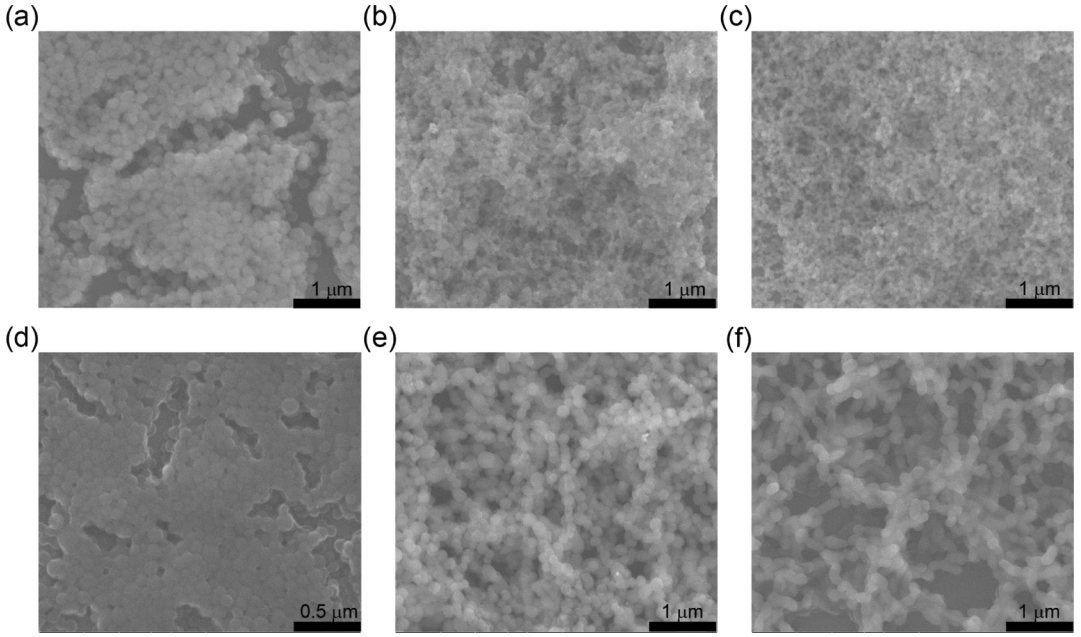

Figure 7. SEM images of **5a** (a), **5b** (b), **5c** (c), **7a** (d), **7b** (e), and **7c** (f) in CH_2Cl_2/hexane mixed solutions with 90% hexane content.

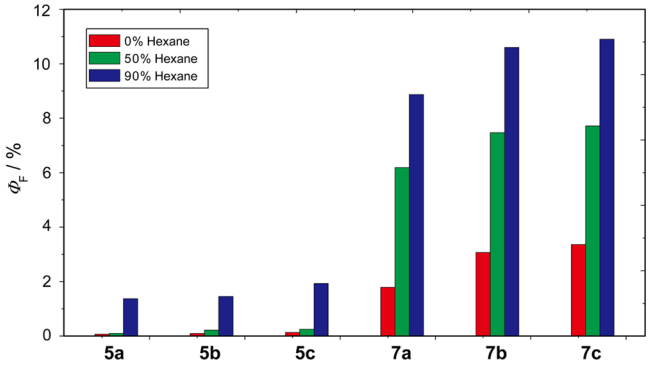

Figure 8. Quantum yields of **5** and **7** versus hexane fraction in CH_2Cl_2/hexane mixtures.

°C. The solvent was then removed in vacuo to give a crude product, which was purified by flash column chromatography (dichloromethane/hexane, 2:1 v/v) to afford **2** as a white solid (0.870 g, 77%). Mp: 189.7−190.5 °C. ^{1}H NMR (CD_2Cl_2, room temperature, 300 MHz, δ, ppm) 7.02−7.13 (m, 14H), 6.58 (d, J = 9.0 Hz, 4H), 1.57−1.78 (m, 24H), 0.93−1.15 (m, 36H). ^{13}C NMR (CD_2Cl_2, room temperature, 75.0 MHz, δ, ppm) 7.78, 14.0, 14.3, 14.5, 125.8, 127.4, 130.8, 131.6, 136.1, 145.1. ^{31}P{^{1}H} NMR (CD_2Cl_2, room temperature, 121.4 MHz, δ, ppm) 12.61 ppm (s, ^{195}Pt satellites, $^1J_{Pt-P}$ = 2772.9 Hz). HR-ESI-MS m/z = 1375.3 for $[M + Na]^+$ $C_{50}H_{78}Br_2NaP_4Pt_2$ and m/z = 1273.4 for $[M - Br]^+$ $C_{50}H_{78}BrP_4Pt_2$.

*Synthesis of **3a**.* Compound **2** (203 mg, 0.150 mmol) and $AgNO_3$ (255 mg, 1.50 mmol) were placed in a 50 mL Schlenk flask followed by 15.0 mL of freshly distilled dichloromethane. The mixture was stirred in the dark at room temperature for 24 h. A clear solution with a heavy creasy precipitate resulted, the precipitate was filtered off, and the solvent was removed under a flow of nitrogen to afford **3a** as a yellow solid (190 mg, 96%). Mp: 241.7−242.9 °C. ^{1}H NMR (CD_2Cl_2, room temperature, 300 MHz, δ, ppm) 6.98−7.12 (m, 14H), 6.57 (d, J = 9.0 Hz, 4H), 1.42−1.56 (m, 24H), 1.01−1.18 (m, 36H). ^{13}C NMR (CD_2Cl_2, room temperature, 75.0 MHz, δ, ppm) 7.46, 12.8, 13.0, 13.2, 125.9, 127.5, 130.8, 131.5, 135.4, 145.0. ^{31}P{^{1}H} NMR (CD_2Cl_2, room temperature, 121.4 MHz, δ, ppm) 19.14 (s, ^{195}Pt satellites, $^1J_{Pt-P}$ = 2895.4 Hz). HR-ESI-MS m/z = 596.2 for $[M - 2NO_3]^{2+}$ $C_{50}H_{78}P_4Pt_2$; m/z calcd for $[M - NO_3]^+$ $C_{50}H_{78}NO_3P_4Pt_2$, 1254.4228, found 1254.3342, error −0.7 ppm.

*Synthesis of **3b**.* Compound **2** (203 mg, 0.150 mmol) and AgOTf (85.0 mg, 0.330 mmol) were placed in a 50 mL Schlenk flask followed by 15.0 mL of freshly distilled dichloromethane. The mixture was stirred in the dark at room temperature for 24 h. A clear solution with a heavy creasy precipitate resulted, the precipitate was filtered off, and the solvent was removed under a flow of nitrogen to afford **3b** as a brown solid (208 mg, 93%). Mp: 204.3−205.2 °C. ^{1}H NMR (CD_2Cl_2, room temperature, 300 MHz, δ, ppm) 6.92−7.14 (m, 14H), 6.54 (d, J = 9.0 Hz, 4H), 1.56−1.79 (m, 24H), 1.03−1.21 (m, 36H). ^{13}C NMR (CD_2Cl_2, room temperature, 100 MHz, δ, ppm) 7.39, 13.6, 125.8, 127.3, 130.6, 131.2, 134.8, 144.4. ^{31}P{^{1}H} NMR (CD_2Cl_2, room temperature, 121.4 MHz, δ, ppm) 20.11 (s, ^{195}Pt satellites, $^1J_{Pt-P}$ = 2845.6 Hz). HR-ESI-MS m/z = 596.2 for $[M - 2OTf]^{2+}$ $C_{50}H_{78}P_4Pt_2$; m/z calcd for $[M - OTf]^+$ $C_{51}H_{78}F_3O_3P_4Pt_2S$, 1341.3870, found 1341.2534, error −1 ppm.

*Self-Assembly of **5a**.* In a 1:1 molar ratio, **3a** (3.95 mg, 3.00 μmol) and **4** (1.46 mg, 3.00 μmol) were dissolved in 600 μL of CH_2Cl_2 in a 2 mL dram vial. The reaction mixture was allowed to stir for 8 h at room temperature. To the resulting homogeneous solution was added diethyl ether to precipitate the product, which was isolated, dried under reduced pressure, and dissolved in CD_2Cl_2 for characterization. ^{1}H NMR (CD_2Cl_2, room temperature, 300 MHz, δ, ppm) 8.51 (d, J = 6.0 Hz, 12H), 7.82 (d, J = 6.0 Hz, 12H), 7.60 (d, J = 9.0 Hz, 12H), 7.19 (d, J = 9.0 Hz, 12H), 6.89−7.13 (m, 72H), 6.67 (d, J = 9.0 Hz, 12H), 1.15−1.36 (m, 72H), 0.91−1.10 (m, 108H). ^{31}P{^{1}H} NMR (CD_2Cl_2, room temperature, 121.4 MHz, δ, ppm) 14.23 (s, ^{195}Pt satellites, $^1J_{Pt-P}$ = 2702.4 Hz). ESI-TOF-MS m/z 839.83 $[M - 6NO_3]^{6+}$, 1020.19 $[M - 5NO_3]^{5+}$, 1290.65 $[M - 4NO_3]^{4+}$, and 1741.21 $[M - 3NO_3]^{3+}$.

*Self-Assembly of **5b**.* In a 1:1 molar ratio, **3b** (4.47 mg, 3.00 μmol) and **4** (1.46 mg, 3.00 μmol) were dissolved in 600 μL of CH_2Cl_2 in a 2 mL dram vial. The reaction mixture was allowed to stir for 8 h at room temperature. To the resulting homogeneous solution was added diethyl ether to precipitate the product, which was isolated, dried under reduced pressure, and dissolved in CD_2Cl_2 for characterization. ^{1}H NMR (CD_2Cl_2, room temperature, 300 MHz, δ, ppm) 8.59 (d, J = 6.0 Hz, 12H), 7.89 (d, J = 6.0 Hz, 12H), 7.68 (d, J = 9.0 Hz, 12H), 7.28 (d, J = 9.0 Hz, 12H), 6.97−7.22 (m, 72H), 6.76 (d, J = 9.0 Hz, 12H), 1.22−1.42 (m, 72H), 0.97−1.16 (m, 108H). ^{31}P{^{1}H} NMR (CD_2Cl_2, room temperature, 121.4 MHz, δ, ppm) 14.27 (s, ^{195}Pt satellites, $^1J_{Pt-P}$ = 2704.8 Hz). ESI-TOF-MS m/z 839.82 [M −

DOI: 10.1021/jacs.6b00846
J. Am. Chem. Soc. 2016, 138, 4580−4588

6OTf]$^{6+}$, 1037.54 [M − 5OTf]$^{5+}$, 1334.32 [M − 4OTf]$^{4+}$, and 1828.01 [M − 3OTf]$^{3+}$.

Synthesis of ***5c***. **5b** (5.93 mg, 1.00 μmol) was dissolved in 500 μL of acetone in a 2 mL dram vial, followed by the addition of a saturated aqueous solution of KPF_6 (500 μL) to precipitate the product. The reaction mixture was centrifuged, washed several times with water, and dried. The pale yellow product **5c** was collected and dissolved in CD_2Cl_2 for characterization. ^{1}H NMR (CD_2Cl_2, room temperature, 300 MHz, δ, ppm) 8.56 (d, *J* = 6.0 Hz, 12H), 7.85 (d, *J* = 6.0 Hz, 12H), 7.65 (d, *J* = 9.0 Hz, 12H), 7.28 (d, *J* = 9.0 Hz, 12H), 7.02−7.22 (m, 72H), 6.76 (d, *J* = 9.0 Hz, 12H), 1.22−1.42 (m, 72H), 0.97−1.16 (m, 108H). ^{31}P{^{1}H} NMR (CD_2Cl_2, room temperature, 121.4 MHz, δ, ppm) 14.27 (s, ^{195}Pt satellites, $^1J_{Pt-P}$ = 2706.0 Hz). ESI-TOF-MS *m*/*z* 1036.73 [M − 5PF_6]$^{5+}$, 1332.07 [M − 4PF_6]$^{4+}$, and 1824.01 [M − 3PF_6]$^{3+}$.

Self-Assembly of ***7a***. In a 2:1 molar ratio, **3a** (7.90 mg, 6.00 μmol) and **6** (1.92 mg, 3.00 μmol) were dissolved in 600 μL of DMSO in a 2 mL dram vial. The reaction mixture was allowed to stir for 8 h at 60 °C. To the resulting homogeneous solution was added toluene to precipitate the product, which was isolated, dried under reduced pressure, and dissolved in DMSO-d_6 for characterization. ^{1}H NMR (DMSO-d_6, room temperature, 300 MHz, δ, ppm) 8.99 (br, 8H), 8.70 (br, 8H), 8.35 (br, 8H), 7.73 (br, 24H), 7.33 (m, 16H), 6.93 (br, 56H), 6.60 (br, 16H), 1.23 (br, 96H), 0.93 (m, 144H). ^{31}P{^{1}H} NMR (DMSO-d_6, room temperature, 121.4 MHz, δ, ppm) 13.66 (s, ^{195}Pt satellites, $^1J_{Pt-P}$ = 2684.2 Hz). ESI-TOF-MS *m*/*z* 1247.25 [M − 5NO_3]$^{5+}$, 1575.27 [M − 4NO_3]$^{4+}$, 2120.27 [M − 3NO_3]$^{3+}$.

Self-Assembly of ***7b***. In a 2:1 molar ratio, **3b** (8.95 mg, 6.00 μmol) and **6** (1.92 mg, 3.00 μmol) were dissolved in 600 μL of DMSO in a 2 mL dram vial. The reaction mixture was allowed to stir for 8 h at 60 °C. To the resulting homogeneous solution was added toluene to precipitate the product, which was isolated, dried under reduced pressure, and dissolved in DMSO-d_6 for characterization. ^{1}H NMR (DMSO-d_6, room temperature, 300 MHz, δ, ppm) 9.00 (br, 8H), 8.71 (br, 8H), 8.35 (br, 8H), 7.74 (br, 24H), 7.34 (m, 16H), 6.95 (br, 56H), 6.61 (br, 16H), 1.24 (br, 96H), 0.94 (m, 144H). ^{31}P{^{1}H} NMR (DMSO-d_6, room temperature, 121.4 MHz, δ, ppm) 13.73 (s, ^{195}Pt satellites, $^1J_{Pt-P}$ = 2695.1 Hz). ESI-TOF-MS *m*/*z* 1058.66 [M − 6OTf]$^{6+}$, 1300.10 [M − 5OTf]$^{5+}$, 1662.13 [M − 4OTf]$^{4+}$, 2264.80 [M − 3OTf]$^{3+}$.

Synthesis of ***7c***. **7b** (6.95 mg, 1.00 μmol) was dissolved in 500 μL of DMSO in a 2 mL dram vial, followed by the addition of a saturated aqueous solution of KPF_6 (500 μL) to precipitate the product. The reaction mixture was centrifuged, washed several times with water, and dried. The yellow product **7c** was collected and dissolved in DMSO-d_6 for characterization. ^{1}H NMR (DMSO-d_6, room temperature, 300 MHz, δ, ppm) 8.97 (br, 8H), 8.70 (br, 8H), 8.34 (br, 8H), 7.74 (br, 24H), 7.32 (br, 16H), 6.84−7.14 (br, 56H), 6.60 (br, 16H), 1.24 (br, 96H), 0.94 (m, 144H). ^{31}P{^{1}H} NMR (DMSO-d_6, room temperature, 121.4 MHz, δ, ppm) 13.74 (s, ^{195}Pt satellites, $^1J_{Pt-P}$ = 2696.3 Hz). ESI-TOF-MS *m*/*z* 1297.91 [M − 5PF_6]$^{5+}$, 1658.16 [M − 4PF_6]$^{4+}$.

■ ASSOCIATED CONTENT

Supporting Information

The Supporting Information is available free of charge on the ACS Publications website at DOI: 10.1021/jacs.6b00846.

Syntheses and characterization data (NMR, ESI-TOF-MS, UV, and FL), including Figures S1−S36, Schemes S1−S7, and Tables S1−S4. (PDF)

X-ray crystallographic data for **2** and **3a**. (CIF)

■ AUTHOR INFORMATION

Corresponding Authors

*x.yan@utah.edu

*fhuang@zju.edu.cn

*stang@chem.utah.edu

Notes

The authors declare no competing financial interest.

■ ACKNOWLEDGMENTS

P.J.S. thanks the NSF (Grant 1212799) for financial support. F.H. thanks the National Basic Research Program (2013CB834502), the NSFC/China (21125417), and the State Key Laboratory of Chemical Engineering for financial support. X.L. thanks the NSF (CHE-1506722) and PREM Center of Texas State University (DMR-1205670) for financial support. Computational resources are gratefully acknowledged from the CHPC at the University of Utah.

■ REFERENCES

(1) (a) Niu, L.-Y.; Guan, Y.-S.; Chen, Y.-Z.; Wu, L.-Z.; Tung, C.-H.; Yang, Q.-Z. *J. Am. Chem. Soc.* **2012**, *134*, 18928. (b) Sun, H.; Liu, S.; Lin, W.; Zhang, K. Y.; Lv, W.; Huang, X.; Huo, F.; Yang, H.; Jenkins, G.; Zhao, Q.; Huang, W. *Nat. Commun.* **2014**, *5*, 3601. (c) Dai, X.; Zhang, Z.; Jin, Y.; Niu, Y.; Cao, H.; Liang, X.; Chen, L.; Wang, J.; Peng, X. *Nature* **2014**, *515*, 96. (d) Yam, V. W.-W.; Au, V. K.-M.; Leung, S. Y.-L. *Chem. Rev.* **2015**, *115*, 7589. (e) Shanmugaraju, S.; Mukherjee, P. S. *Chem. - Eur. J.* **2015**, *21*, 6656. (f) Chowdhury, A.; Howlader, P.; Mukherjee, P. S. *Chem. - Eur. J.* **2016**, *22*, 1424.

(2) (a) Luo, J.; Xie, Z.; Lam, J. W. Y.; Cheng, L.; Chen, H.; Qiu, C.; Kwok, H. S.; Zhan, X.; Liu, Y.; Zhu, D.; Tang, B. Z. *Chem. Commun.* **2001**, 1740. (b) Mei, J.; Hong, Y.; Lam, J. W. Y.; Qin, A.; Tang, Y.; Tang, B. Z. *Adv. Mater.* **2014**, *26*, 5429. (c) Mei, J.; Leung, N. L. C.; Kwok, R. T. K.; Lam, J. W. Y.; Tang, B. Z. *Chem. Rev.* **2015**, *115*, 11718.

(3) Zhao, Z.; Lam, J. W. Y.; Tang, B. Z. *J. Mater. Chem.* **2012**, *22*, 23726.

(4) (a) Shustova, N. B.; McCarthy, B. D.; Dincă, M. *J. Am. Chem. Soc.* **2011**, *133*, 20126. (b) Wei, Z.; Gu, Z.-Y.; Arvapally, R. K.; Chen, Y.-P.; McDougald, R. N., Jr; Ivy, J. F.; Yakovenko, A. A.; Feng, D.; Omary, M. A.; Zhou, H.-C. *J. Am. Chem. Soc.* **2014**, *136*, 8269. (c) Wang, P.; Yan, X.; Huang, F. *Chem. Commun.* **2014**, *50*, 5017. (d) Zhao, J.; Yang, D.; Zhao, Y.; Yang, X.-J.; Wang, Y.-Y.; Wu, B. *Angew. Chem., Int. Ed.* **2014**, *53*, 6632. (e) Peng, H.-Q.; Xu, J.-F.; Chen, Y.-Z.; Wu, L.-Z.; Tung, C.-H.; Yang, Q.-Z. *Chem. Commun.* **2014**, *50*, 1334.

(5) (a) Fujita, M.; Tominaga, M.; Hori, A.; Therrien, B. *Acc. Chem. Res.* **2005**, *38*, 369. (b) Oliveri, C. G.; Ulmann, P. A.; Wiester, M. J.; Mirkin, C. A. *Acc. Chem. Res.* **2008**, *41*, 1618. (c) De, S.; Mahata, K.; Schmittel, M. *Chem. Soc. Rev.* **2010**, *39*, 1555. (d) Chakrabarty, R.; Mukherjee, P. S.; Stang, P. J. *Chem. Rev.* **2011**, *111*, 6810. (e) Cook, T. R.; Zheng, Y.-R.; Stang, P. J. *Chem. Rev.* **2013**, *113*, 734. (f) Wang, M.; Wang, C.; Hao, X.-Q.; Liu, J.; Li, X.; Xu, C.; Lopez, A.; Sun, L.; Song, M.-P.; Yang, H.-B.; Li, X. *J. Am. Chem. Soc.* **2014**, *136*, 6664. (g) Cook, T. R.; Stang, P. J. *Chem. Rev.* **2015**, *115*, 7001. (h) Brown, C. J.; Toste, F. D.; Bergman, R. G.; Raymond, K. N. *Chem. Rev.* **2015**, *115*, 3012. (i) Newkome, G. R.; Moorefield, C. N. *Chem. Soc. Rev.* **2015**, *44*, 3954. (j) McConnell, A. J.; Wood, C. S.; Neelakandan, P. P.; Nitschke, J. R. *Chem. Rev.* **2015**, *115*, 7729. (k) Sun, B.; Wang, M.; Lou, Z.; Huang, M.; Xu, C.; Li, X.; Chen, L.-J.; Yu, Y.; Davis, G. L.; Xu, B.; Yang, H.-B.; Li, X.-P. *J. Am. Chem. Soc.* **2015**, *137*, 1556.

(6) (a) Inokuma, Y.; Kawano, M.; Fujita, M. *Nat. Chem.* **2011**, *3*, 349. (b) Yan, X.; Li, S.; Pollock, J. B.; Cook, T. R.; Chen, J.; Zhang, Y.; Ji, X.; Yu, Y.; Huang, F.; Stang, P. J. *Proc. Natl. Acad. Sci. U. S. A.* **2013**, *110*, 15585. (c) Yan, X.; Jiang, B.; Cook, T. R.; Zhang, Y.; Li, J.; Yu, Y.; Huang, F.; Yang, H.-B.; Stang, P. J. *J. Am. Chem. Soc.* **2013**, *135*, 16813. (d) Li, Z.-Y.; Zhang, Y.; Zhang, C.-W.; Chen, L.-J.; Wang, C.; Tan, H.; Yu, Y.; Li, X.; Yang, H.-B. *J. Am. Chem. Soc.* **2014**, *136*, 8577. (e) Li, S.; Huang, J.; Zhou, F.; Cook, T. R.; Yan, X.; Ye, Y.; Zhu, B.; Zheng, B.; Stang, P. J. *J. Am. Chem. Soc.* **2014**, *136*, 5908. (f) Yan, X.; Xu, J.-F.; Cook, T. R.; Huang, F.; Yang, Q.-Z.; Tung, C.-H.; Stang, P. J. *Proc. Natl. Acad. Sci. U. S. A.* **2014**, *111*, 8717. (g) Yamashina, M.; Sartin, M. M.; Sei, Y.; Akita, M.; Takeuchi, S.; Tahara, T.; Yoshizawa, M. *J. Am. Chem. Soc.* **2015**, *137*, 9266. (h) Roy, B.; Ghosh, A. K.; Srivastava, S.;

DOI: 10.1021/jacs.6b00846
J. Am. Chem. Soc. 2016, 138, 4580−4588

D'Silva, P.; Mukherjee, P. S. *J. Am. Chem. Soc.* **2015**, *137*, 11916. (i) Kaphan, D. M.; Levin, M. D.; Bergman, R. G.; Raymond, K. N.; Toste, F. D. *Science* **2015**, *350*, 1235. (j) Lee, H.; Elumalai, P.; Singh, N.; Kim, H.; Lee, S. U.; Chi, K.-W. *J. Am. Chem. Soc.* **2015**, *137*, 4674.
(7) (a) Kaloudi-Chantzea, A.; Karakostas, N.; Raptopoulou, C. P.; Psycharis, V.; Saridakis, E.; Griebel, J.; Hermann, R.; Pistolis, G. *J. Am. Chem. Soc.* **2010**, *132*, 16327. (b) Pollock, J. B.; Schneider, G. L.; Cook, T. R.; Davies, A. S.; Stang, P. J. *J. Am. Chem. Soc.* **2013**, *135*, 13676. (c) Yan, X.; Cook, T. R.; Wang, P.; Huang, F.; Stang, P. J. *Nat. Chem.* **2015**, *7*, 342. (d) Chen, L.-J.; Ren, Y.-Y.; Wu, N.-W.; Sun, B.; Ma, J.-Q.; Zhang, L.; Tan, H.; Liu, M.; Li, X.; Yang, H.-B. *J. Am. Chem. Soc.* **2015**, *137*, 11725. (e) Yan, X.; Wang, H.; Hauke, C. E.; Cook, T. R.; Wang, M.; Saha, M. L.; Zhou, Z.; Zhang, M.; Li, X.; Huang, F.; Stang, P. J. *J. Am. Chem. Soc.* **2015**, *137*, 15276.
(8) (a) Hofmeister, F. *Naunyn-Schmiedeberg's Arch. Pharmacol.* **1888**, *24*, 247. (b) Klaus, A.; Tiddy, G. J. T.; Rachel, R.; Trinh, A. P.; Maurer, E.; Touraud, D.; Kunz, W. *Langmuir* **2011**, *27*, 4403.
(9) Zhou, X.; Li, H.; Chi, Z.; Zhang, X.; Zhang, J.; Xu, B.; Zhang, Y.; Liu, S.; Xu, J. *New J. Chem.* **2012**, *36*, 685.
(10) Kapadia, P.; Widen, J. C.; Magnus, M. A.; Swenson, D. C.; Pigge, F. C. *Tetrahedron Lett.* **2011**, *52*, 2519.
(11) Yoshida, T.; Matsuda, T.; Otsuka, S.; Parshall, G. W.; Peet, W. G. *Inorg. Synth.* **1990**, *28*, 122.

DOI: 10.1021/jacs.6b00846
J. Am. Chem. Soc. 2016, 138, 4580−4588